Title

The Role of Cholesterol and Structurally Related Molecules in Enhancing Transfection of Cationic Liposome–DNA Complexes

Journal

The Journal of Physical Chemistry B, 113(15)

ISSN

1520-6106

Authors

Zidovska, Alexandra

Evans, Heather M

Ahmad, Ayesha

et al.

Publication Date

2009-04-16

DOI

10.1021/jp809000e

Published in final edited form as:
J Phys Chem B. 2009 April 16; 113(15): 5208–5216. doi:10.1021/jp809000e.

The Role of Cholesterol and Structurally Related Molecules in Enhancing Transfection by Cationic Liposome–DNA Complexes

Alexandra Zidovska, **Heather M. Evans**, **Ayesha Ahmad**, **Kai K. Ewert**, and **Cyrus R. Safinya***
Materials, Physics, and Molecular, Cellular and Developmental Biology Departments, University of California at Santa Barbara, Santa Barbara, CA 93106, USA

Abstract

Motivated by its important role in gene delivery, we have studied the effect of cholesterol and analogs on the transfection efficiency (TE) of lamellar cationic liposome–DNA (CL–DNA) complexes in vitro. Addition of cholesterol to low-transfecting DOTAP/DOPC–DNA complexes increases TE, with 15 mol% cholesterol already yielding tenfold improvement. Steroids lacking the alkyl tail only modestly enhance TE, while molecules retaining it strongly enhance TE. All steroid-containing CL–DNA complexes retain the lamellar structure. The increase in experimentally determined membrane charge density (a universal parameter governing TE of lamellar CL–DNA complexes) with cholesterol content alone can not account for the rapid increase of TE. Instead, the reduction of the hydration repulsion layer of the membrane, caused by replacement of DOPC by cholesterol, promotes fusion between cationic membranes of CL–DNA complexes and anionic endosomal membranes, thus facilitating release of complexes and enhancing TE.

Keywords

Cationic Liposome–DNA complexes; charged membranes; cholesterol; steroids; sterols; transfection

Introduction

Cationic liposomes (CLs) have attracted a lot of scientific interest over the past two decades as their advantages as gene delivery vectors were recognized and they became the most prevalent synthetic carriers (vectors) of genes worldwide[1-4]. The major benefits of CLs for gene delivery are the ability to transfer DNA of unlimited size (enabling transfer of large human genes and even artificial chromosomes; in contrast, viral capsids can carry a maximum of about 40 kbp) and the ease of preparation (since the vector is formed spontaneously by self-assembly[5-7]). There is ongoing extensive research activity to overcome the major drawback of CL-vectors, which is their low transfection efficiency (TE, a measure of the ability to transfer DNA into a cell followed by gene expression) compared to viral vectors[2,3]. For this purpose, numerous lipid formulations have been systematically studied [8,9]. They typically contain a combination of cationic and neutral (helper) lipids such as DOPE or cholesterol. Lipid mixtures for successful transfection in vivo seem to require cholesterol, but this phenomenon is not understood[10]. Several reports in the literature claim that DOPE, while successfully used for in vitro gene delivery, is a poor helper lipid for in vivo applications[11-15]. Cholesterol has also been included in liposomes along with cationic DOTAP and fusogenic DOPE to form a potent

* Corresponding author: Materials Research Laboratory, University of California, Santa Barbara, CA, 93106, Phone: 805-893 8635, Fax: 805-893 7221, E-mail: E-mail: safinya@mrl.ucsb.edu.

Supporting Information Available: Fig. 5 and Fig. 10 including standard deviations for all TE measurements. This material is available free of charge via the Internet at http://pubs.acs.org.

mixture used to study the treatment of ovarian cancer by delivery of the p53 tumor suppressor gene[16,17].

The goal of the present work is to help to elucidate our discovery of an unexpectedly large enhancement of the TE of cationic lipid–DNA (CL–DNA) complexes upon incorporation of cholesterol. The starting point of this investigation are CLs comprised of DOTAP and DOPC. The structure and transfection behavior of these CL–DNA complexes have been studied previously [5-8,18,19]. We have investigated the effect of added cholesterol and structurally related molecules (β-estradiol, ergosterol, ergocalciferol, dihydroisoandrosterone and progesterone) in the low-transfecting regime of the DOTAP/DOPC–DNA system[18,19]. In particular, we attempted to determine the structure-function relationship of the CL–DNA complexes containing cholesterol or other structurally related molecules. While keeping the charge (corresponding to the molar fraction of cationic lipid, here monovalent DOTAP) constant, we gradually replaced DOPC molecules by cholesterol. Employing structural studies via X-ray diffraction and transfection efficiency measurements, we were able to uncover the correlation between the TE and structure of these cholesterol-containing CL–DNA complexes in vitro. TE increases by a factor of ten with the inclusion of only 15 mol% cholesterol, and further inclusion of cholesterol continues to increase TE.

X-ray diffraction confirms that DOTAP/DOPC–DNA complexes retain the lamellar structure upon addition of cholesterol and other structurally related molecules. Previous work has identified the membrane charge density (σ_M) as a universal parameter for TE of lamellar, DOPC containing CL–DNA complexes[18-20], with TE following a bell-shaped curve as a function of σ_M[19]. These studies further demonstrated that upon endocytosis CL–DNA complexes were trapped within endosomes at low σ_M[18]. The nearly exponential increase of TE with increasing σ_M was attributed to a kinetic barrier for endosomal fusion, with increases in σ_M decreasing the barrier. For cholesterol-containing charged membranes however, the changes in σ_M alone, experimentally determined via XRD, cannot explain the unexpectedly rapid increase of TE with cholesterol content. We have shown that the reduction of the average hydration repulsion layer of the membrane, caused by replacement of DOPC by cholesterol, is crucial for the exponential TE enhancement. This suggests that decreased hydration leads to reduced hydration repulsion and thus enhanced fusion of the cationic membranes of CL–DNA complexes with the anionic membrane of the endosome, facilitating endosomal release. Thus, our findings suggest that suppression of hydration repulsion, independent from the effect of σ_M on the kinetic barrier for endosomal fusion, also reduces that barrier. Steroid molecules that are more hydrophilic than cholesterol and lacking the alkyl tail (such as β-estradiol, progesterone and dehydroisoandrosterone) only modestly enhance TE. In contrast, analogs retaining the alkyl chain (ergosterol and ergocalciferol) give large TE enhancements similar to cholesterol, even when the polycyclic steroid framework is disrupted as in ergocalciferol.

Materials and Methods

Lipid Solutions

1,2-dioleoyl-*sn*-glycero-3-phosphocholine (DOPC) and 1,2-dioleoyl-3-trimethylammonium-propane (DOTAP) were purchased as solutions in chloroform from Avanti Polar Lipids. Cholesterol, ergosterol, ergocalciferol, β-estradiol, progesterone, dihydroisoandrosterone and PC-cholesterol were purchased in powder form from Sigma Aldrich, and dissolved in chloroform to prepare stock solutions. Lipid solutions were combined at the desired ratio of lipids and dried, first by a stream of nitrogen and subsequently in a vacuum for 8 to 12 hours. To the residue, high conductivity (18.2 MΩ) water was added and the mixture was incubated at 37 °C for at least 12 hours to give solutions of a final concentration of 30 m_M for X-ray samples. For transfection, solutions were prepared at 0.6 m_M. Lipid mixtures containing higher

molar fractions of DOPC formed opaque suspensions, which were sonicated to clarity and filtered through 0.2 μm filters. The lipid solutions were stored at 4 °C until use.

Optical Microscopy

A Nikon Diaphot 300 inverted microscope equipped for epifluorescence and differential interference contrast (DIC) and a SensiCam^{QE} High Speed digital camera were used. A Nikon Optiphot-2Pol microscope was used for polarized microscopy. We observed lipid mixtures prepared for transfection studies at 0.6 m_M. The samples were first checked for birefringence by polarized microscopy, and then studied by DIC microscopy.

Transfection

Mouse fibroblast cells L-cells (CCL-1) were a gift from C. Samuel (UCSB). Cells were cultured at 37 °C in supplemented cell medium (Dulbecco's Modified Eagle's Medium (DMEM) with 1% penicillin-streptomycin and 5% fetal bovine serum, v/v; from Gibco BRL) in an atmosphere containing 5% CO_2 and reseeded approximately every 72 hours to maintain sub-confluency. The day before the transfection experiment, cells were seeded in 24-well plates. At the time of transfection, the cells were approximately 70% confluent. Luciferase plasmid DNA (pGL3 Control Vector, Promega) was prepared using a Qiagen Giga Kit (Qiagen). For each well, 1 μg of luciferase plasmid DNA was used. Lipid solution (0.6 m_M total lipid at lipid/DNA charge ratio of 2.8) was added to the DNA and the mixture was diluted to a final volume of 0.5 ml with non-supplemented DMEM. This mixture was allowed to incubate for 15 minutes. The cells were incubated with this solution for six hours, rinsed three times with Phosphate Buffered Saline (PBS, Invitrogen) and incubated with supplemented cell media for an additional 24 hours. Luciferase gene expression was measured with the Luciferase Assay System (Promega) and light output readings were taken on a Berthold AutoLumat luminometer. Transfection efficiency, measured as relative light units (RLU), was normalized to the weight of total cellular protein determined using Bio-Rad Protein Assay Dye Reagent (Bio-Rad). TE experiments (of two independent TE measurements per data point) with cholesterol were performed 6 times; TE experiments with ergosterol, ergocalciferol, progesterone and dehydroisoandrosterone were performed 4 times; and TE experiments with β-estradiol and PC-cholesterol were performed 2 times over a period of one year. All experiments included a measurement of a reference sample consisting of 30 Mol% DOTAP and 70 Mol% DOPC used for normalization of the obtained data. The data was then averaged over all experiments and the standard deviation computed.

Small Angle X-ray Scattering

Lipid solution (see above) was added to 0.2 mg of highly polymerized calf thymus DNA (HPCT, from USB; prepared at 5 mg/ml in water). Samples were centrifuged for 2.5 hours at 19,000 RPM in a Sorvall SS34 rotor and stored at 4 °C for at least two days to reach equilibrium. Typically, the CL–DNA complexes formed a white precipitate and these pellets were transferred to 1.5 mm quartz capillaries and flame sealed. X-ray scattering data was collected at beamline 4-2 of the Stanford Synchrotron Radiation Laboratory (SSRL) during four runs, over the course of two years. The X-ray scattering patterns were reproducible between samples on different runs. The beam energy was 8.98 keV and the distance of the sample to the detector was 1 m. A charge-coupled device-based area detector (MarCCD165, Mar USA, Evanston, IL) was used. Silver behenate was used as a calibration standard. X-ray scattering data was collected for 5 min (no radiation damage occurred in sample during this time). The acquired radial scattering patterns were integrated over 360° to obtain plots of scattering intensity versus momentum transfer. All displayed X-ray data was automatically corrected for beam intensity fluctuations by the data acquisition software in use at the synchrotron source.

Results and Discussion

Transfection Efficiency of DOTAP/DOPC/Cholesterol CL–DNA Complexes

Fig. 1 A shows the transfection efficiency of CL–DNA complexes composed of a binary lipid mixture of monovalent DOTAP and neutral helper lipid DOPC (*circles*). The TE of this system increases over several orders of magnitude as the molar fraction of cationic lipid (DOTAP) increases. As reported earlier, DOTAP/DOPC CL–DNA complexes form the highly organized lamellar L_α^c phase[6]. In this structure, lipid bilayers alternate with layers of DNA in a sandwich-like fashion. The TE of these lamellar CL–DNA complexes is strongly dependent on the membrane charge density σ_M, unlike the TE of DOPE containing hexagonal CL–DNA complexes, which is known to be independent of the membrane charge density of the CL–DNA complex. This phenomenon suggests that there are different transfection mechanisms/pathways for CL–DNA complexes of distinct structures, which was confirmed by confocal microscopy by Lin et al[18].

We held the charge of the system constant by keeping the DOTAP content in the DOTAP/DOPC CL–DNA complexes unchanged. Furthermore, we prepared all samples at a constant $\Phi_{DOTAP} = 0.3$, and gradually replaced DOPC molecules by cholesterol molecules. A different individual sample was prepared for each specific composition of the ternary lipid mixture (DOTAP/DOPC/cholesterol). As shown in Fig. 1B (markers of different shapes correspond to different $\Phi_{cholesterol}$, see legend in Fig. 1 A), TE of the ternary lipid mixture DOTAP/DOPC/cholesterol increases by a factor of ten with the addition of only 15 mol% cholesterol, and further addition of cholesterol continues to increase the TE. Thus, TE strongly depends on the cholesterol molar fraction. A direct comparison of TE levels of the binary lipid mixture DOTAP/DOPC (*circles*) and the ternary lipid mixture DOTAP/DOPC/cholesterol (*grey markers*) as a function of cationic lipid content is displayed in Fig. 1A. Addition of cholesterol results in an exponential enhancement of TE without increasing the charge of the lipid mixture (the amount of cationic lipid is constant).

Structure Determination of CL–DNA Complexes via Small Angle X-ray Scattering

A possible explanation for the dramatic increase in the TE of DOTAP/DOPC CL–DNA complexes upon addition of cholesterol is a phase transition from the lamellar phase towards a different, highly transfecting phase. However, X-ray diffraction shows that the lamellar structure of the DOTAP/DOPC–DNA complexes is retained upon addition of cholesterol. Fig. 2 A shows small angle X-ray scattering data for DOTAP/DOPC/cholesterol–DNA complexes, where $\Phi_{DOTAP} = 0.3$ and DOPC molecules are gradually being replaced by cholesterol molecules ($\Phi_{DOPC} + \Phi_{cholesterol} = 0.7$). The structure of these CL–DNA complexes remains lamellar as cholesterol content increases. First and second order of the lamellar peak are marked by q_{001} and q_{002}. Black arrow heads point to the DNA peak at q_{DNA}. At $\Phi_{cholesterol} \geq 0.4$, phase coexistence of CL–DNA complexes and cholesterol monohydrate crystals is observed (q_{chol}, marked by grey arrows).

From the X-ray data the lamellar spacing d ($d = 2\pi/q_{001} = \delta_m + d_w$, where δ_m is the membrane thickness and d_w is the thickness of water layer) as well as the spacing between the DNA molecules d_{DNA} ($= 2\pi/q_{DNA}$) can be obtained[6]. Fig. 2 B shows the variation of d_{DNA} with cholesterol content at the isoelectric point of the CL–DNA complex (lipid/DNA charge ratio = 1). At the isoelectric point, d_{DNA} allows calculation of the membrane charge density of the lipid bilayer, because the negative charge of DNA has to neutralize the positive charge on the adjacent lipid bilayers[6,21]. Simple geometrical arguments, taking the lamellar geometry of the CL–DNA complex into account, yield:

$$\sigma_M = e/(d_{DNA} \cdot 3.4\ \text{Å}) \quad (1)$$

where e is the elementary charge and 3.4 Å corresponds to the bare distance between two charges along a DNA molecule. Therefore, the DNA spacing obtained by X-ray diffraction is a direct experimental measurement of the membrane charge density of lamellar CL–DNA complexes. A decrease in d_{DNA} from 63 Å to 29 Å with increasing cholesterol content thus signifies an increase of the membrane charge density. This is expected, because the headgroup area of cholesterol ($A_{cholesterol}$ = 40 Å^2) is smaller than that of DOPC (A_{DOPC} = 72 Å^2), thus reducing the total membrane area[22,23]. As the total membrane area shrinks while the membrane charge, given by Φ_{DOTAP} = 0.3, remains constant, the membrane charge density necessarily increases. Fig. 2 C displays the intralamellar spacing of cholesterol-containing CL–DNA complexes. The lamellar spacing first rises from 70 Å to 72 Å and then drops to 65 Å as a function of increasing cholesterol content.

As observed with X-ray diffraction, there is a transition from a single-phase regime (where all cholesterol is incorporated into the lipid bilayer) to a multiphase regime (excess cholesterol coexists with CL–DNA complexes as cholesterol monohydrate crystals) at $\Phi_{cholesterol}$ = 0.4 (cf. Fig. 2 B & C). This is in agreement with previous reports in the literature which also observe membrane saturation with cholesterol at about 40 mol%[24,25]. This implies a reduction of the molar fraction of cholesterol in the membrane and thus a change in membrane composition, most notably of Φ_{DOTAP}. We will address this issue in detail below.

Membrane Charge Density: Experiment vs. Theory

Recent work has identified the membrane charge density σ_M as a universal parameter for TE of lamellar, DOPC containing CL–DNA complexes[18-20], with TE following a bell-shaped curve as a function of σ_M. Given the fact that cholesterol-containing CL–DNA complexes accommodate the lamellar structure, it is instructive to plot the TE of these complexes against σ_M to check whether they follow the universal behavior shown by Ahmad et al.[19]. We have determined the membrane charge density both experimentally and theoretically (Fig. 3 A). Fig. 3 A (*squares*) shows the membrane charge density experimentally obtained from X-ray diffraction data using Eq.1. A particularly strong increase in σ_M is apparent for $\Phi_{cholesterol} \geq$ *0.4*, where the system enters the multiphase regime.

Fig. 3 A (*triangles*) shows σ_M resulting from our theoretical calculations. These calculations of membrane charge density use

$$\sigma_M = eZ\Phi_{DOTAP}/(\Phi_{DOTAP}A_{DOTAP} + \Phi_{DOPC}A_{DOPC} + \Phi_{cholesterol}\ A_{cholesterol}) \quad (2)$$

where $\Phi_{DOTAP/DOPC/cholesterol}$ is the molar fraction of DOTAP, DOPC or cholesterol, respectively; Z is the valence of DOTAP (Z = 1); and $A_{DOTAP/DOPC/cholesterol}$ is the headgroup area (cross-sectional area per lipid) of DOTAP, DOPC or cholesterol, respectively. As elaborated below, we used $A_{cholesterol}$ = 40 Å^2, A_{DOPC} = 63.3 Å^2, and A_{DOTAP} = 60.4 Å^2. In addition, our calculation assumes membrane saturation with cholesterol at $\Phi_{cholesterol}$ = 0.4, independent of membrane composition. This means that for lipid mixtures of an initial $\Phi_{cholesterol} \geq 0.4$, there is only $\Phi_{cholesterol}$ = 0.4 in the membrane because the remaining cholesterol crystallizes as cholesterol monohydrate. Thus, the effective Φ_{DOTAP} in membrane (which was constant at Φ_{DOTAP} = 0.3 in all initial lipid mixtures) increases. Φ_{DOTAP} increases from Φ_{DOTAP} = 0.3 for $\Phi_{cholesterol}$ = 0.4 to Φ_{DOTAP} = 0.6 for an initial $\Phi_{cholesterol}$ = 0.7, thus

contributing to the increase of σ_M. In this regime, Φ_{DOPC} is calculated from mass balance as $\Phi_{DOPC} = 1 - \Phi_{DOTAP} - \Phi_{cholesterol} = 0.6 - \Phi_{DOTAP}$.

The headgroup area of cholesterol was assumed to be constant, independent of the membrane composition ($A_{cholesterol}$ = 40 Å^2)[22]. This is a reasonable presumption considering the rigid structure of the cholesterol molecule. The headgroup areas for DOPC and DOTAP were determined by a combined experimental and theoretical approach as follows. For a binary mixture of a cationic and a zwitterionic lipid such as DOPC, it has been shown previously in calculations based on Poisson-Boltzmann theory[26,27] as well as in related experimental systems (i.e. DMPC/DMTAP monolayers[28]) that the value of the headgroup area of the zwitterionic lipid passes a minimum with increasing molar fraction of the charged lipid. This is due to changes in the orientation of the P-N dipole of the phosphatidylcholine headgroup caused by the electric field of the charged lipids. The effective electric field is strongly dependent on the amount of charged lipid in the membrane. The headgroup area of the zwitterionic lipid reaches a broad minimum at roughly an equimolar lipid mixture. In analogy to the calculations of Gurtovenko et al.[27] for DMTAP/DMPC mixtures, we have calculated the headgroup area for DOPC in the binary mixture with DOTAP. We have used an initial A_{DOPC} = 72 Å^2 for Φ_{DOPC} = 1 and Φ_{DOTAP} = 0 to estimate A_{DOPC} for Φ_{DOTAP} = 0.3-0.6, which is the interval relevant for our experiments. We find that A_{DOPC} is roughly constant at 63.3 Å^2 for Φ_{DOTAP} = 0.3-0.6. Using this value of A_{DOPC}, we finally calculated A_{DOTAP} from Eq. 2, using σ_M obtained by X-ray diffraction (Eq. 1) of CL–DNA complexes at Φ_{DOTAP} = 0.3 and Φ_{DOPC} = 0.7 ($\Phi_{cholesterol}$ = 0). This yields A_{DOTAP} = 60.4 Å^2.

As evident from Fig. 3 A, the calculated (*triangles*) and experimentally (*squares*) obtained σ_M agree well, supporting our assumptions. To further analyse the membrane charge density data, we have calculated A_{DOTAP} from Eq. 2 using the experimentally obtained σ_M, A_{DOPC} = 63.27 Å^2 and $A_{cholesterol}$ = 40 Å^2. Fig. 3 B shows the ratio $r = A_{DOTAP}/A_{DOPC}$, illustrating the variation of A_{DOTAP} with increasing $\Phi_{cholesterol}$. The nonmonotonical changes in r with membrane composition may be explained by considering the absolute electrostatic interaction between zwitterionic DOPC and monovalent DOTAP, a mechanism proposed by Gurtovenko et al.[27] At low molar fractions of DOTAP, the reorientation of the P-N dipoles of DOPC leads to a tight packing of alternating DOTAP and DOPC laterally compressing the bilayer. The fact that DOPC is gradually replaced by the smaller and more rigid cholesterol then explains the initial decrease in r for $\Phi_{cholesterol} \leq 0.4$. For $\Phi_{cholesterol} \geq 0.4$, Φ_{DOTAP} significantly increases as explained above. This corresponds to an increasing number of neighboring cationic DOTAP molecules, which electrostatically repel each other. Thus, the distances between the DOTAP molecules increase, effectively increasing their headgroup area.

TE and Membrane Charge Density

Fig. 4 shows the TE of DOTAP/DOPC/cholesterol–DNA complexes (*empty circles*) plotted as a function of experimentally obtained σ_M. TE of the ternary DOTAP/DOPC/cholesterol lipid mixture shows a significantly different behavior as observed for binary systems, which follow a universal bell shaped curve as a function of the σ_M[19]. TE of cholesterol-containing CL–DNA complexes dramatically increases more than two orders of magnitude with increasing cholesterol content, while holding the charge (Φ_{DOTAP}) constant. An exponential TE enhancement can be observed for $0 < \Phi_{cholesterol} \leq 0.4$, no further TE increase is seen for $\Phi_{cholesterol} > 0.4$ (here, membrane is saturated with cholesterol, $\Phi_{chol,\ membrane} = 0.4 = const.$). The changes in the membrane charge density σ_M alone (as discussed above) cannot explain such a significant increase in TE. A possible explanation for this TE increase, however, could be the overall reduction of the hydration repulsion layer of the membrane, when DOPC gets replaced by cholesterol. The hydration repulsion layer is a strongly bound and oriented layer of water molecules at the surfaces.[29] If the hydration layers of two surfaces overlap, the

arrangement of the water molecules in the hydration layer is disturbed and an exponentially repulsive force arises. It is known that the hydration repulsion layer of cholesterol is much smaller compared to DOPC[29,30]. Therefore, when we exchange DOPC by cholesterol, we reduce the average membrane hydration layer leading to reduced repulsion and thus to enhanced fusion[29]. In other words, the CL–DNA complexes would more readily fuse with the endosomal membrane, facilitating endosomal release and increasing the probability of a successful transfection. After the membrane saturation with cholesterol has been reached ($\Phi_{\text{cholesterol}} > 0.4$, but $\Phi_{\text{chol, membrane}} = 0.4 = \text{const.}$), there is no further reduction of the hydration repulsion layer. TE seems to remain around its maximum value. As we discussed earlier, there is a significant increase in Φ_{DOTAP} for $\Phi_{\text{cholesterol}} \geq 0.4$, which results in a significant increase of σ_M.

Structurally Related Molecules: Steroids and Ergocalciferol

To investigate the structural basis for the TE improvement upon addition of cholesterol, we have studied molecules structurally related to cholesterol such as sterols (ergosterol, β-estradiol), other steroids (progesterone and dihydroisoandrosterone) and ergocalciferol, which derives from a steroid precursor by opening of a central ring. The TEs of DOTAP/DOPC–DNA complexes containing these molecules are shown in Fig. 5 A. Two distinct trends can be observed. The data for ergosterol and ergocalciferol seems to show a dependence of TE on the steroid content similar to that of cholesterol: TE monotonically increases with the increasing molar fraction of steroid, leading to dramatic improvements in TE. In contrast, when β-estradiol, progesterone and dihydroisoandrosterone are incorporated into CL–DNA complexes, TE increases only very slightly as a function of their molar fraction until high steroid contents (35 mol% and higher) are reached, where TE suddenly increases to values comparable with TE data for cholesterol. The only deviation from this behavior is seen at small (5 and 10 mol%) contents of dihydroisoandrosterone, where the averaged TE data for this steroid is very similar to that of cholesterol. However, the error in the data is large and the data at higher sterol contents (which is more relevant for applications) strongly suggests grouping the steroids as listed above. The major structural differences between the two groups are the absence of the short alkyl chain attached to the hydrophobic core and the presence of a second polar moiety on the other end of the molecule (attached to the five-membered ring of the core) in case of β-estradiol, progesterone and dihydroisoandrosterone. The chemical structures of the studied molecules are presented in Fig. 5 B.

We have characterized the structural properties of CL–DNA complexes containing steroids and ergocalciferol using X-ray diffraction. Fig. 6 shows a summary of X-ray diffraction data for ergosterol (Fig. 6 A) and ergocalciferol (Fig. 6 B). The data for DOTAP/DOPC complexes containing ergosterol (Fig. 6 A) shows that their structure remains lamellar with increasing $\Phi_{\text{ergosterol}}$ (first and second order of the lamellar peak are marked by q_{001} and q_{002}). For $\Phi_{\text{ergosterol}} \geq 0.4$, ergosterol crystals are observed (q_{ergo}, marked by grey arrows). Black arrowheads point to the DNA peak at q_{DNA}. In case of ergocalciferol, the X-ray diffraction data (Fig. 6 B) reveals a more complex behavior: at $\Phi_{ergocalciferol} = 0.1$, the structure of the CL–DNA complexes is lamellar (first and second order of the lamellar peak are marked by q_{001} and q_{002}), however, for $\Phi_{\text{ergocalciferol}} \geq 0.2$, a second lamellar phase occurs (first and second order of its lamellar peak are marked by black arrows). At $\Phi_{\text{ergocalciferol}} \geq 0.4$, coexistence of ergocalciferol crystals can be observed (q_{ec}, marked by grey arrows), suggesting membrane saturation with ergocalciferol. Black arrow heads point to the DNA peak at q_{DNA}.

Fig. 7 shows a summary of small angle X-ray scattering data for DOTAP/DOPC complexes containing β-estradiol (Fig. 7 A), progesterone (Fig. 7 B) or dihydroisoandrosterone (Fig. 7 C), labeled as the data in Fig. 6. The structure of these CL–DNA complexes remains lamellar for all Φ_{steroid} studied. Both q_{002} and q_{DNA} can be discerned for all membrane compositions,

as demonstrated in Fig. 7 F, which shows an enlargement of the boxed section of Fig. 7 C. No peaks corresponding to steroid crystals are visible in the X-ray diffraction data. This is due to the low density of the crystals of β-estradiol, progesterone and dihydroisoandrosterone which macroscopically phase separate from the CL–DNA complexes during sample preparation by centrifugation. However, crystals of these steroids are observed at $\Phi_{steroid} \geq 0.3$ by polarized microscopy as shown in Fig. 7 D and Fig. 7 E for progesterone and dehydroisoandrosterone. The structural features of β-estradiol, progesterone and dihydroisoandrosterone, i.e., absence of an alkyl tail and the presence of a second polar group, seem to favor crystallization at lower molar fractions of steroid compared to cholesterol.

From the X-ray diffraction data, we have obtained the lamellar repeat distance d and d_{DNA} of the CL–DNA complexes. As shown in Fig. 8 A, the DNA spacing d_{DNA} monotonically decreases from 63 Å to 27 Å for all studied steroids. However, d_{DNA} in CL–DNA complexes containing cholesterol and ergosterol is always about 1-2 Å larger than d_{DNA} in CL–DNA complexes containing β-estradiol, progesterone or dihydroisoandrosterone. Fig. 8 B shows the lamellar repeat distance d of CL–DNA complexes containing steroids. For cholesterol and ergosterol, d is generally up to 5 Å higher than for the other steroids, suggesting a different packing of these groups of molecules within the lipid bilayer. This is also supported by our observation that β-estradiol, progesterone and dihydroisoandrosterone crystallize at lower $\Phi_{steroid}$ than cholesterol and ergosterol. Ergocalciferol was not included in this structural analysis because two lamellar phases coexist for $\Phi_{ergocalciferol} \geq 0.3$

Fig. 9 shows the TEs of the DOTAP/DOPC/steroid–DNA complexes plotted as a function of σ_M. The membrane charge densities were obtained from X-ray diffraction data using Eq. 1. The data for cholesterol (*dark circles*) and ergosterol (*dark triangles*) deviate significantly from the universal TE curve (*black solid line*), whereas the TE data for progesterone (*grey triangles*) and dehydroisoandrosterone (*grey circles*) nearly follow the universal behavior. The interpretation of the TE data for DOTAP/DOPC/cholesterol–DNA complexes was discussed earlier and we expect it to hold for ergosterol as well, due to very similar results in transfection as well as X-ray diffraction experiments. On the other hand, CL–DNA complexes containing progesterone and dehydroisoandrosterone show different behavior in transfection or X-ray diffraction experiments, even though they likely reduce the average hydration repulsion layer of the membrane in the same way as cholesterol. A possible explanation for this phenomenon is that these steroid molecules enhance the repulsion of the membranes because of increased protrusion forces. Both progesterone and dehydroisoandrosterone possess two polar groups which dictate a positioning of the molecules close to the water interface (due to their increased hydrophilicity). The resulting protrusion forces seem to cancel the benefits of the reduced hydration repulsion layer with respect to the activated fusion with the endosomal membrane.

In order to test our hypothesis that the reduction of the hydration repulsion layer by cholesterol is responsible for the enhancement of TE, we have performed transfection experiments with DNA complexes of a ternary mixture of DOTAP, DOPC and a cholesterol derivative, PC-cholesterol (cholesteryl-phosphatidylcholine), in which the hydroxyl group of cholesterol has been replaced by a phosphatidylcholine group. The chemical structure of PC-cholesterol is shown in Fig. 10 B. The headgroups of PC-cholesterol and DOPC are essentially identical, thus having a similar (if not identical) hydration repulsion layer. Fig. 10 A compares the TE of DNA-complexes of DOTAP/DOPC/cholesterol (*black squares*) and DOTAP/DOPC/PC-cholesterol lipid mixtures (*grey markers*). CL–DNA complexes containing PC-cholesterol do not show any enhancement of TE with increasing PC-cholesterol content. This is strong evidence that the reduction of the hydration repulsion layer is, indeed, crucial for the TE enhancement.

Prior work has found that CL–DNA complexes at low σ_M remain trapped within endosomes after endocytosis[18]. The nearly exponential increase of TE with increasing σ_M has been attributed to a kinetic barrier for endosomal fusion, with increases in σ_M decreasing the barrier. Other parameters, such as the membrane bending rigidity κ and the membrane Gaussian modulus κ_G, were predicted to impact the energy barrier height[18]. Our findings reported here have identified the hydration repulsion layer of the cationic membranes of CL–DNA complexes as a further parameter contributing to the kinetic barrier for endosomal fusion. The hydration layer decreases as the molar fraction of the cholesterol in the membrane increases, leading to a reduced hydration repulsion and thus enhanced fusion of the cationic membranes of CL–DNA complexes with the anionic membrane of the endosome. This facilitates endosomal release, which strongly increases the probability of successful transfection.

Conclusions

Cholesterol is one of the most studied molecules of all times, and yet it still provides us with many unexplained phenomena. The biological significance of cholesterol stems from its involvement in numerous cellular mechanisms and processes. In the cell, cholesterol is essential for the structure and maintenance of membranes (regulating the fluidity and viscosity of the membrane), cell metabolism (aiding the digestion of fat soluble vitamins), numerous biochemical processes (as a precursor in the synthesis of steroid hormones, bile and vitamin D), signaling and endocytosis (essential for the structure and function of invaginated caveolae and clathrin-coated pits). As we reported here, cholesterol also plays a key role in lipid-based gene delivery, enhancing the TE of certain lipid-based vectors by more than a factor of 100. In this work, we have established a correlation between the effect of cholesterol on TE in vitro and the structural changes it induces in CL–DNA complexes. This correlation can be explained in terms of an increase of the membrane charge density and a reduction of the membrane hydration repulsion layer, utilizing the universal TE curve introduced earlier by Ahmad et al[19]. Prior work has found that CL–DNA complexes at low σ_M remain trapped within endosomes after endocytosis[18]. The nearly exponential increase of TE with increasing σ_M has been attributed to a kinetic barrier for endosomal fusion, with increases in σ_M decreasing the barrier. We have shown here that the hydration repulsion layer of the cationic membrane of CL–DNA complexes is another parameter contributing to the kinetic barrier for endosomal fusion. The hydration layer decreases as the molar fraction of the cholesterol in the membrane increases, leading to a reduced hydration repulsion and thus enhanced fusion of the cationic membranes of CL–DNA complexes with the anionic membrane of the endosome. This facilitates endosomal release and therefore strongly increases the probability of successful transfection.

Supplementary Material

Refer to Web version on PubMed Central for supplementary material.

Acknowledgments

This work was supported by NIH GM-59288 and NSF-DMR 0803103. The X-ray diffraction work was carried out at the Stanford Synchrotron Radiation Laboratory which is supported by the Department of Energy.

References

1. Felgner PL, Gadek TR, Holm M, Roman R, Chan HW, Wenz M, Northrop JP, Ringold GM, Danielsen M. Proc Natl Acad Sci USA 1987;84:7413. [PubMed: 2823261]
2. Huang, L.; Hung, MC.; Wagner, E. Non-Viral Vectors for Gene Therapy. Vol. 2nd. Vol. 53. Elsevier; San Diego: 2005.
3. Ewert KK, Ahmad A, Evans HM, Safinya CR. Expert Opin Biol Ther 2005;5:33. [PubMed: 15709908]

4. http://www.wiley.co.uk/genetherapy/clinical/.
5. Koltover I, Salditt T, Radler JO, Safinya CR. Science 1998;281:78. [PubMed: 9651248]
6. Radler JO, Koltover I, Salditt T, Safinya CR. Science 1997;275:810. [PubMed: 9012343]
7. Ewert KK, Evans HM, Zidovska A, Bouxsein NF, Ahmad A, Safinya CR. J Am Chem Soc 2006;128:3998. [PubMed: 16551108]
8. Miller AD. Curr Med Chem 2003;10:1195. [PubMed: 12678794]
9. Oliver M, Jorgensen MR, Miller A. Tetrahedron Lett 2004;45:3105.
10. Ilies MA, Johnson BH, Makori F, Miller A, Seitz WA, Thompson EB, Balaban AT. Arch Biochem Biophys 2005;435:217. [PubMed: 15680924]
11. Song YK, Liu F, Chu SY, Liu DX. Hum Gene Ther 1997;8:1585. [PubMed: 9322091]
12. Liu Y, Mounkes LC, Liggitt HD, Brown CS, Solodin I, Heath TD, Debs RJ. Nat Biotechnol 1997;15:167. [PubMed: 9035144]
13. Audouy S, Molema G, de Leij L, Hoekstra D. J Gen Med 2000;2:465.
14. Crook K, Stevenson BJ, Dubouchet M, Porteous DJ. Gene Ther 1998;5:137. [PubMed: 9536275]
15. Li S, Tseng WC, Stolz DB, Wu SP, Watkins SC, Huang L. Gene Ther 1999;6:585. [PubMed: 10476218]
16. Kim CK, Haider KH, Choi SH, Choi EJ, Ahn WS, Kim YB. Gynecologic Oncology 2002;84:85. [PubMed: 11748982]
17. Kim CK, Choi EJ, Choi SH, Park JS, Haider KH, Ahn WS. Gynecologic Oncology 2003;90:265. [PubMed: 12893186]
18. Lin AJ, Slack NL, Ahmad A, George CX, Samuel CE, Safinya CR. Biophys J 2003;84:3307. [PubMed: 12719260]
19. Ahmad A, Evans HM, Ewert K, George CX, Samuel CE, Safinya CR. J Gen Med 2005;7:739.
20. Ewert K, Ahmad A, Evans HM, Schmidt HW, Safinya CR. J Med Chem 2002;45:5023. [PubMed: 12408712]
21. Koltover I, Salditt T, Safinya CR. Biophys J 1999;77:915. [PubMed: 10423436]
22. Slotte JP, Jungner M, Vilcheze C, Bittman R. Biochim Biophys Acta, Biomembr 1994;1190:435.
23. Tristram-Nagle S, Petrache HI, Nagle JF. Biophys J 1998;75:917. [PubMed: 9675192]
24. Epand RM, Hughes DW, Sayer BG, Borochov N, Bach D, Wachtel E. Biochim Biophys Acta, Biomembr 2003;1616:196.
25. Huang JY, Buboltz JT, Feigenson GW. Biochim Biophys Acta, Biomembr 1999;1417:89.
26. Mbamala EC, Fahr A, May S. Langmuir 2006;22:5129. [PubMed: 16700604]
27. Gurtovenko AA, Patra M, Karttunen M, Vattulainen I. Biophys J 2004;86:3461. [PubMed: 15189847]
28. Zantl R, Baicu L, Artzner F, Sprenger I, Rapp G, Radler JO. J Phys Chem B 1999;103:10300.
29. Israelachvili, JN. Intermolecular and Surface Forces. Vol. Second edition. Academic Press; London: 1992.
30. Petrache HI, Harries D, Parsegian VA. Macromolecular Symposia 2004;219:39.

Abbreviations

CL
cationic lipid

TE
transfection efficiency

DOTAP
1,2-dioleoyl-3-trimethylammonium-propane

DOPE
1,2-dioleoyl-*sn*-glycero-3-phosphatidylethanolamine

DOPC

1,2-dioleoyl-*sn*-glycero-3-phosphatidylcholine

DIC

differential interference contrast

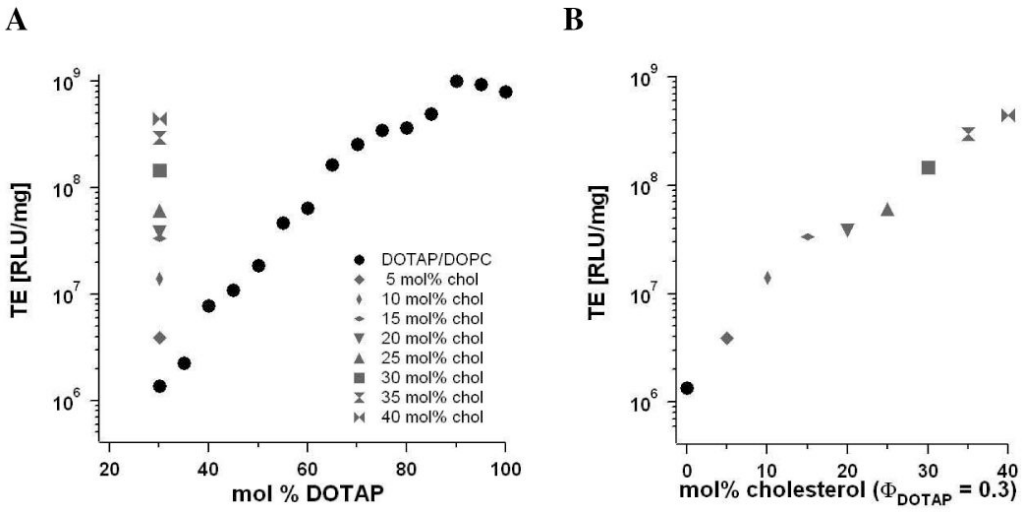

Figure 1.

(A) TE of DNA complexes of binary DOTAP/DOPC lipid mixtures *(black circles)*. Their TE increases over several orders of magnitude with increasing molar fraction of monovalent DOTAP (Φ_{DOTAP}). Grey symbols represent TE of DNA complexes of ternary DOTAP/DOPC/cholesterol lipid mixtures with constant $\Phi_{DOTAP} = 0.3$. Different symbol shapes correspond to different $\Phi_{cholesterol}$ (cf. legend). (B) The TE for the ternary DOTAP/DOPC/cholesterol lipid mixture ($\Phi_{DOPC} + \Phi_{cholesterol} = 0.7$), plotted as a function of $\Phi_{cholesterol}$. The increase of TE with $\Phi_{cholesterol}$ is essentially exponential.

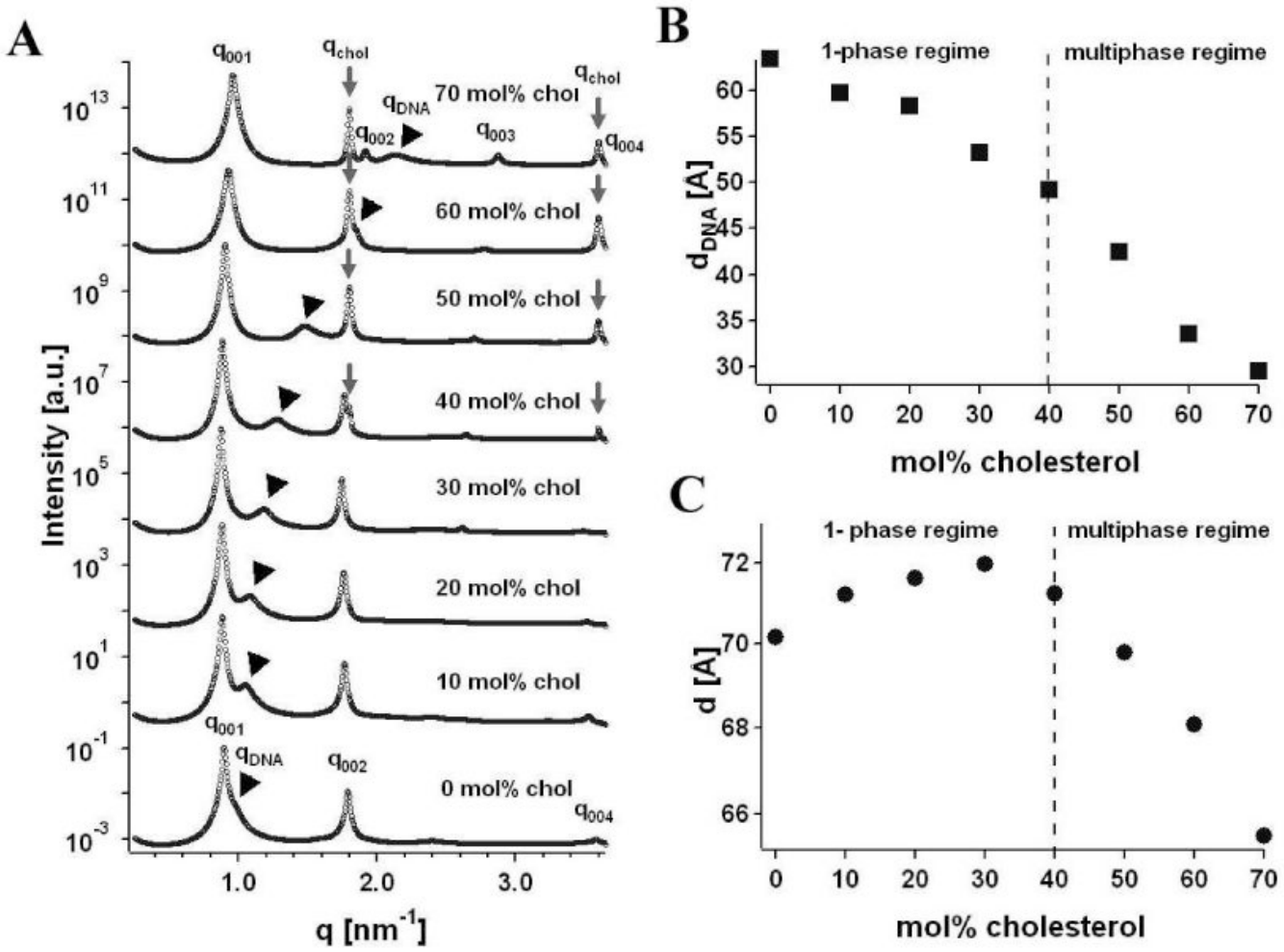

Figure 2.

(A) Small-angle X-ray scattering data for DOTAP/DOPC/cholesterol–DNA complexes, where $\Phi_{DOTAP} = 0.3$ and DOPC is gradually replaced by cholesterol ($\Phi_{DOPC} + \Phi_{cholesterol} = 0.7$). The structure of these CL–DNA complexes remains lamellar with increasing $\Phi_{cholesterol}$ (first and second order of the lamellar peak are marked by q_{001} and q_{002}). At $\Phi_{cholesterol} \geq 0.4$, phase coexistence of CL–DNA complexes and cholesterol monohydrate crystals is observed (q_{chol}, marked by grey arrows). Black arrowheads point to the DNA peak at q_{DNA}. (B) The interaxial spacing between DNA molecules (d_{DNA}) obtained from X-ray scattering data acquired at the isoelectric point of the CL–DNA complexes. At this point (lipid/DNA charge ratio = 1), d_{DNA} is directly correlated with the membrane charge density of the lipid bilayer because the negative charge of DNA precisely neutralizes the positive charge on the adjacent lipid bilayers. (C) Lamellar spacing d of cholesterol-containing CL–DNA complexes obtained from X-ray scattering data. The lamellar spacing rises from 70 Å to 72 Å and then drops to 65 Å as a function of increasing cholesterol content. In B and C, the transition from single-phase regime (all cholesterol is incorporated in the membrane) to multiphase regime (coexistence of CL–DNA complexes and cholesterol monohydrate crystals) is marked by a dashed line.

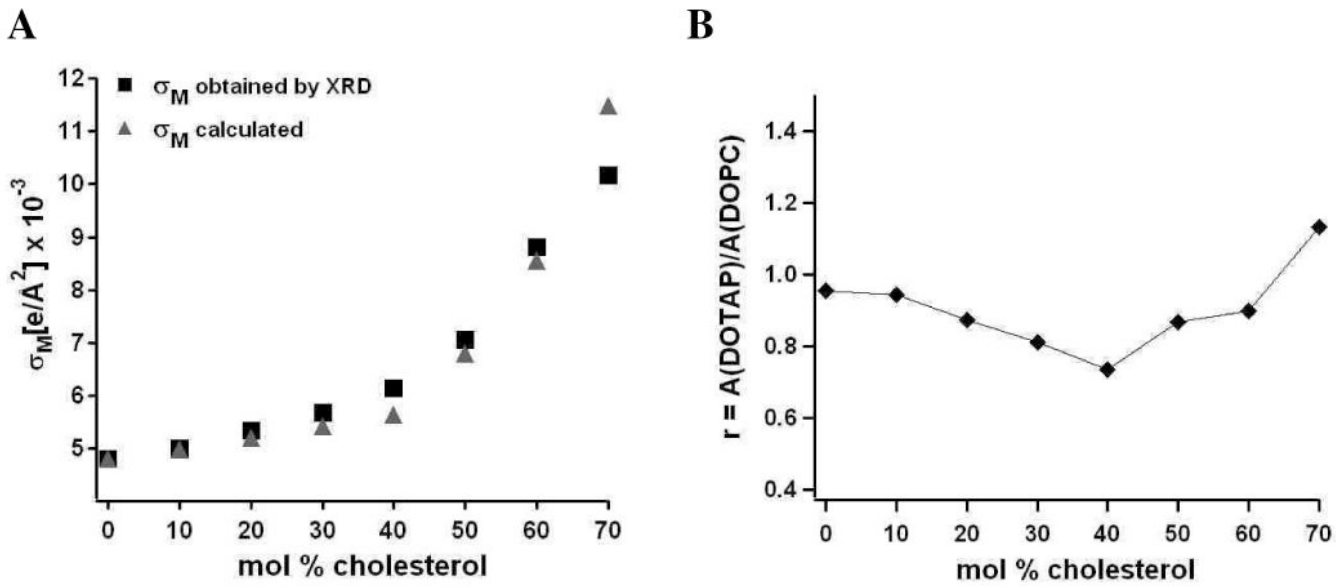

Figure 3.

(A) The membrane charge density σ_M of DOTAP/DOPC/cholesterol–DNA complexes: The squares show σ_M obtained experimentally from X-ray diffraction data, using Eq.1 and the values of d_{DNA} shown in Fig. 2 B. The triangles show σ_M as calculated according to Eq.2, taking membrane saturation with cholesterol at $\Phi_{cholesterol} = 0.4$ into account as described in the text. (B) The ratio $r = A_{DOTAP}/A_{DOPC}$, plotted against $\Phi_{cholesterol}$, illustrates the variation in A_{DOTAP} with increasing $\Phi_{cholesterol}$.

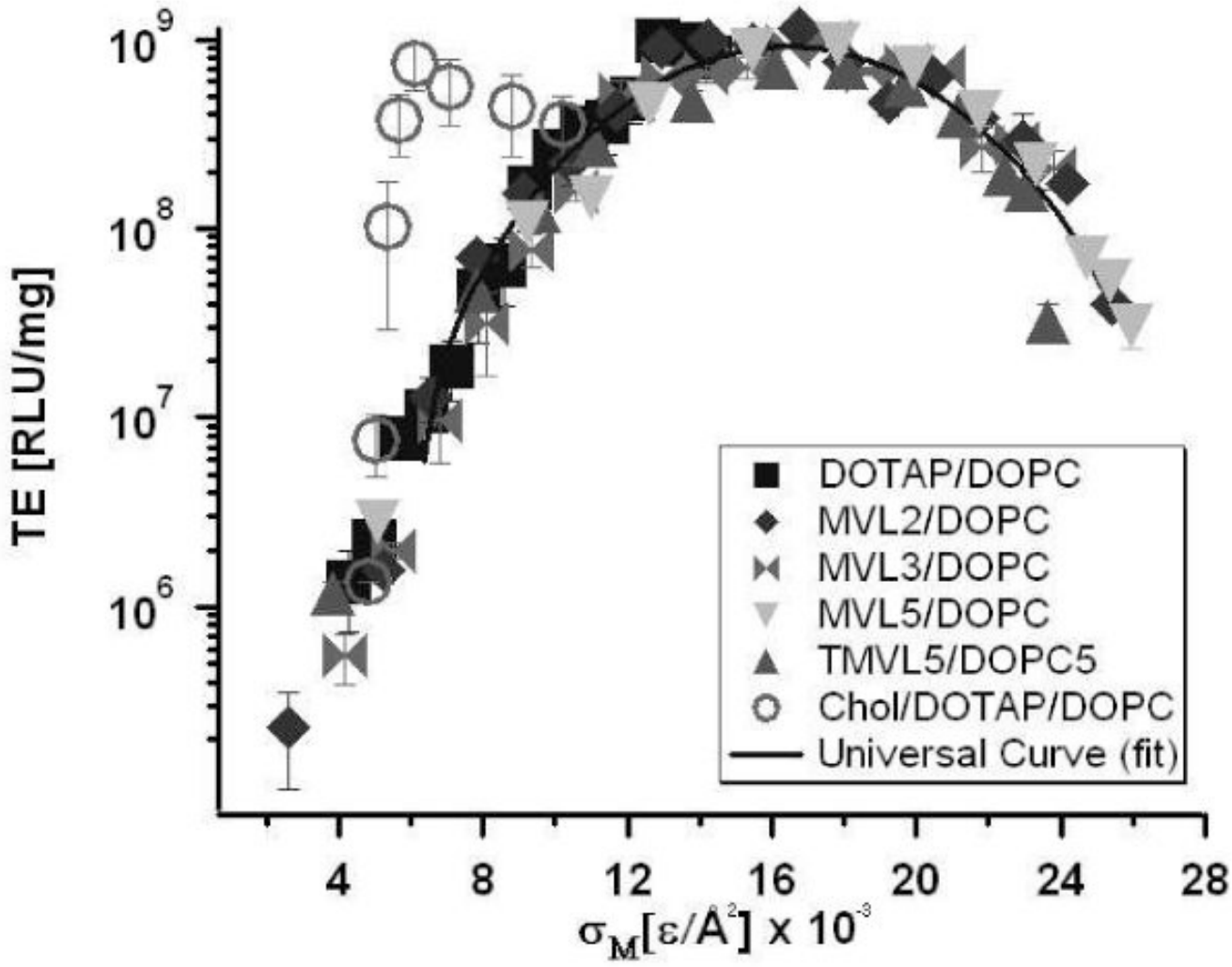

Figure 4.
The TE of the DNA complexes of ternary DOTAP/DOPC/cholesterol lipid mixtures (*empty circles*) plotted against σ_M significantly deviates from the universal bell shaped curve observed for binary systems[19].

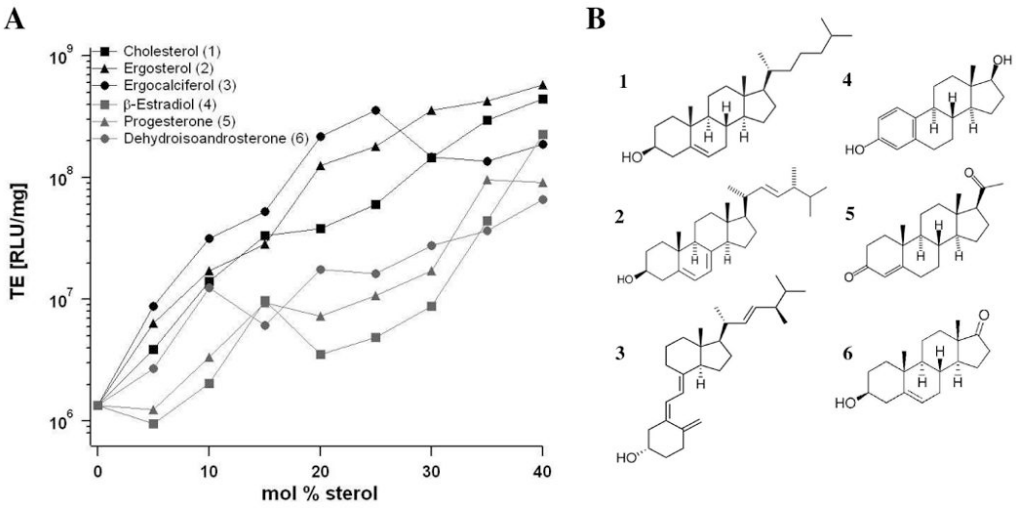

Figure 5.

(A) TEs of DOTAP/DOPC/steroid–DNA complexes. The TE data for ergosterol **2** and ergocalciferol **3** follows a similar dependence on the steroid content in the membrane as that of cholesterol **1**: TE rapidly increases with $\Phi_{steroid}$. In contrast, addition of β-estradiol **4**, progesterone **5** and dehydroisoandrosterone **6** only modestly enhances TE until high steroid contents (35 mol% and higher) are reached, where phase separation occurs (cf. Fig. 7) and TE suddenly increases to values comparable with TE of cholesterol-containing complexes. The major structural differences between these two groups of molecules are the absence of the terminal alkyl chain and the presence of a second polar moiety in case of **4–6.** (B) Chemical structure of the investigated steroid molecules.

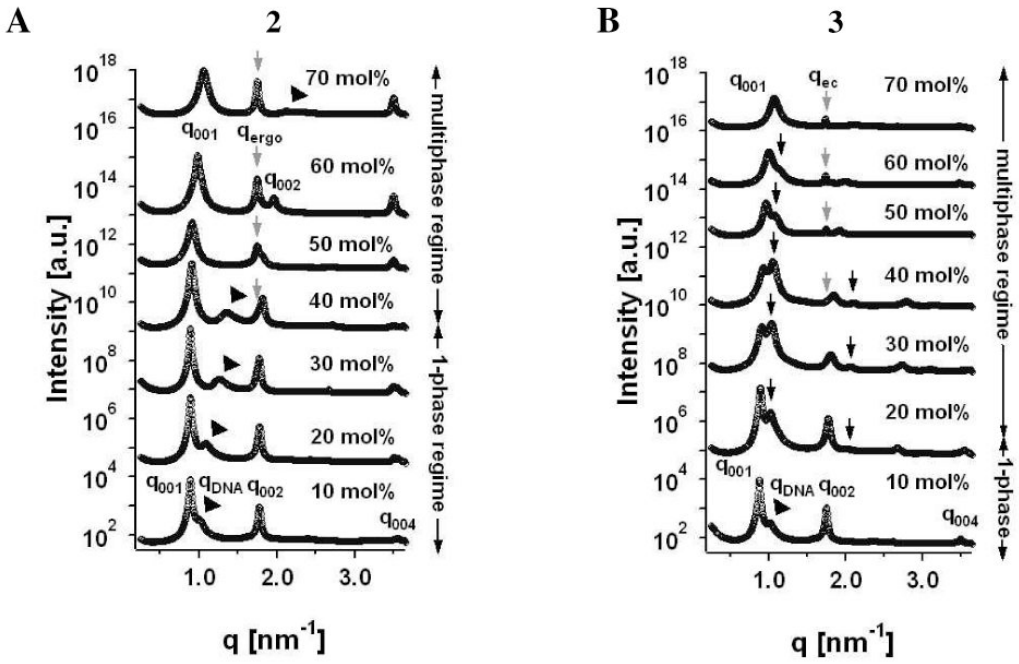

Figure 6.

(A) Small-angle X-ray scattering data for DOTAP/DOPC/ergosterol–DNA complexes shows that their structure remains lamellar with increasing $\Phi_{ergosterol}$ (first and second order of the lamellar peak are marked by q_{001} and q_{002}). At $\Phi_{\text{ergosterol}} \geq 0.4$, ergosterol crystals coexist with CL–DNA complexes (q_{ergo}, marked by grey arrows). Black arrowheads point to the DNA peak at q_{DNA}. (B) X-ray diffraction data for DOTAP/DOPC/ergocalciferol–DNA complexes shows that at $\Phi_{\text{ergocalciferol}} = 0.1$, their structure is lamellar (first and second order of the lamellar peak are marked by q_{001} and q_{002}). For $\Phi_{\text{ergocalciferol}} \geq 0.2$, a second lamellar phase is observed (first and second order of its lamellar peak are marked by black arrows). At $\Phi_{\text{ergocalciferol}} \geq 0.4$, ergocalciferol crystals coexist with CL–DNA complexes (q_{ec}, marked by grey arrows). Black arrowheads point to the DNA peak at q_{DNA}.

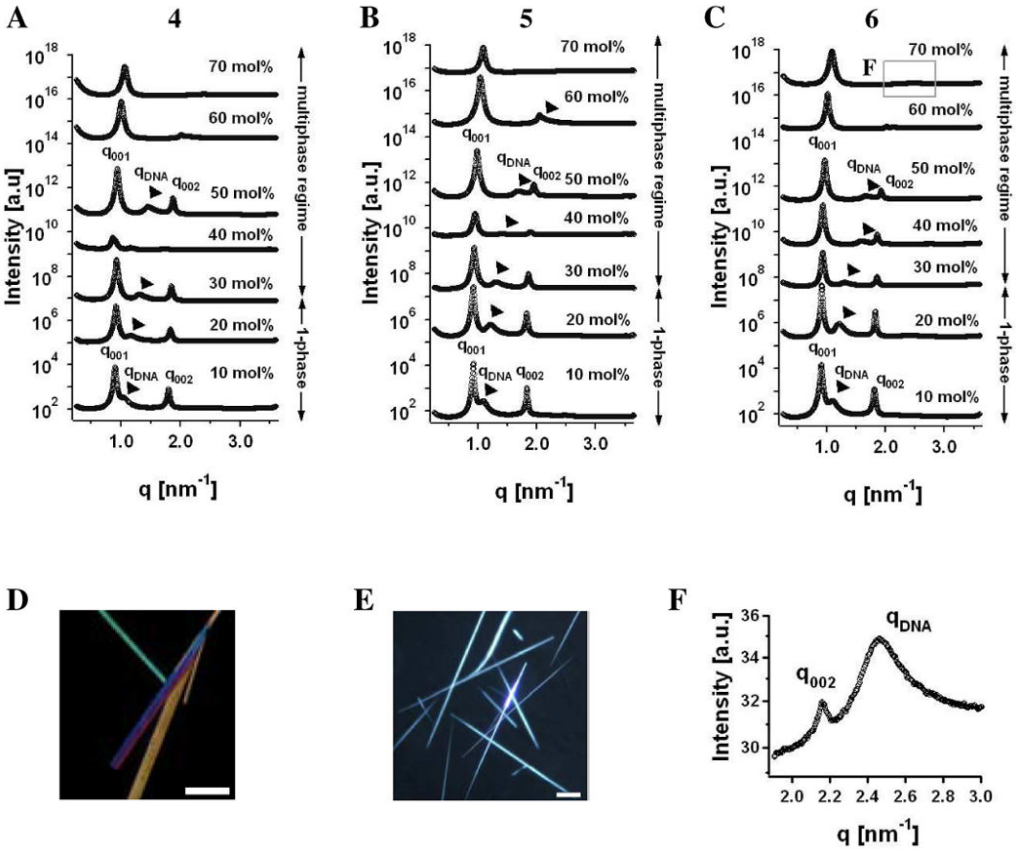

Figure 7.

Small-angle X-ray scattering data for DOTAP/DOPC/steroid–DNA complexes containing β-estradiol (A), progesterone (B) or dihydroisoandrosterone (C) show that the structure of these complexes retains lamellar for all $\Phi_{steroid}$ studied (first and second harmonic order of the lamellar peaks are marked by q_{001} and q_{002}). Black arrowheads point to the DNA peak at q_{DNA}. No diffraction from steroid crystals is observed in the X-ray diffraction data, since they macroscopically separate from the CL–DNA complexes during sample preparation by centrifugation due to their low density. However, polarized microscopy demonstrates that steroid crystals coexist with CL–DNA complexes at $\Phi_{steroid} \geq 0.3$. Examples of progesterone crystals and dehydroisoandrosterone crystals are shown in (D) and (E), respectively. (F) An enlarged view of the boxed section from (C) clearly shows the presence of the second order lamellar peak (q_{001}) as well as the DNA peak at q_{DNA}.

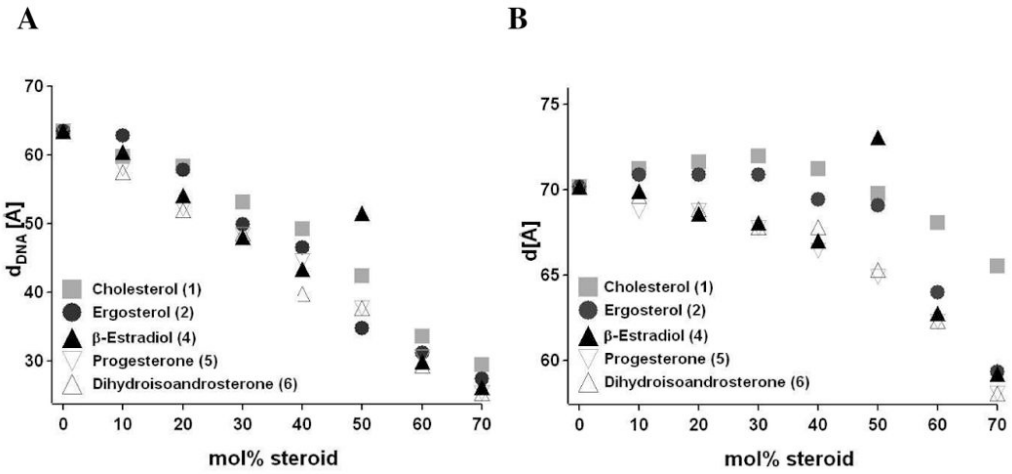

Figure 8.

(A) Values of d_{DNA} for DOTAP/DOPC/steroid–DNA complexes obtained from X-ray diffraction data. There is no significant difference in d_{DNA} for the different steroids, and the DNA spacing monotonically decreases from 63 Å to 27 Å for all studied molecules. However, d_{DNA} of CL–DNA complexes containing cholesterol and ergosterol is always about 1–2 Å larger than d_{DNA} of CL–DNA complexes containing β-estradiol, progesterone or dehydroisoandrosterone. (B) The lamellar spacing *d* of DOTAP/DOPC/steroid–DNA complexes obtained from X-ray diffraction data. The lamellar spacing is generally up to 5 Å higher for CL–DNA complexes containing cholesterol and ergosterol than for complexes containing the other steroids, suggesting different packing of these groups of molecules within the lipid bilayer.

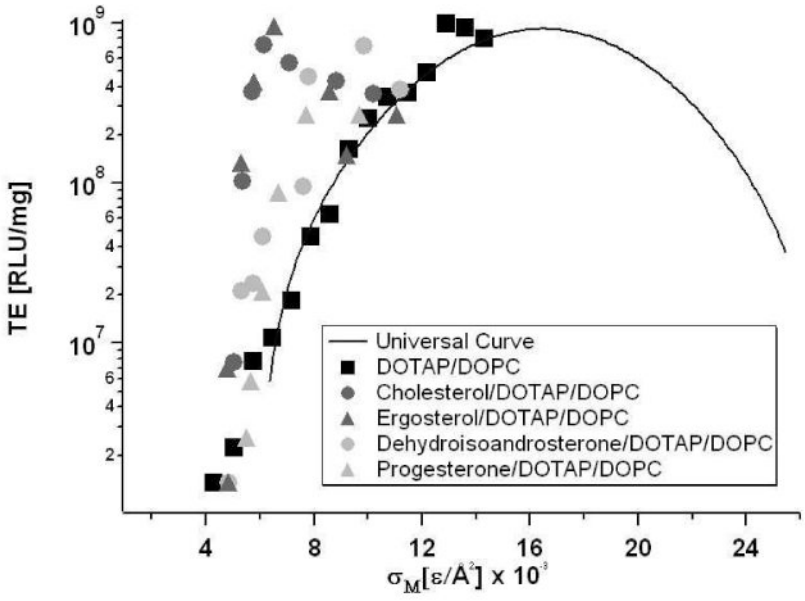

Figure 9.

TEs of DOTAP/DOPC/steroid–DNA complexes plotted as a function of experimentally obtained σ_M. The data for cholesterol (*dark circles*) and ergosterol (*dark triangles*) deviate significantly from the universal TE curve (*black solid line*), whereas the TE data for progesterone (*grey triangles*) and dehydroisoandrosterone (*grey circles*) nearly follow the universal behavior.

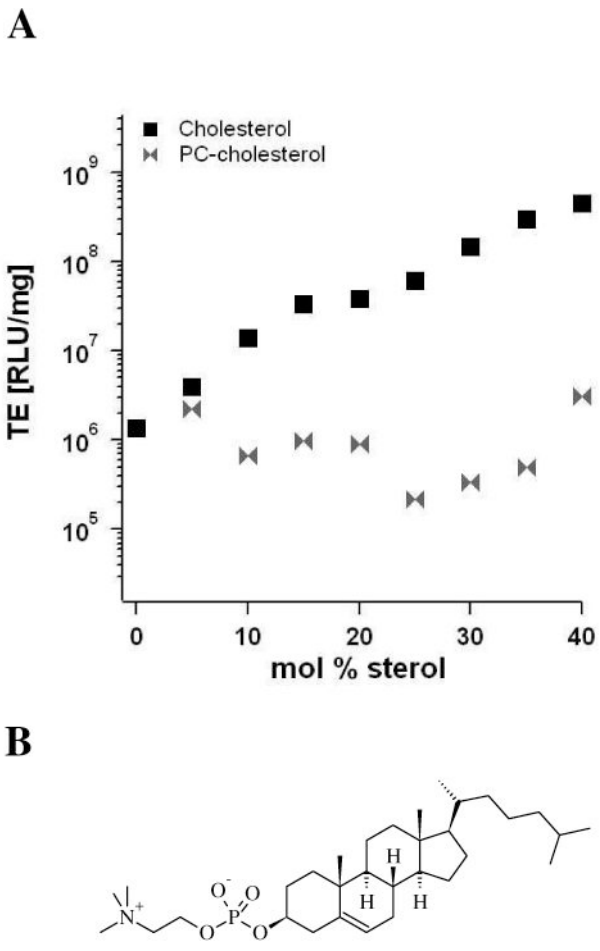

Figure 10.

(A) A comparison of the TE of DOTAP/DOPC/cholesterol–DNA complexes (*black squares*) and DOTAP/DOPC/PC-cholesterol–DNA complexes (*grey markers*). The replacement of DOPC with PC-cholesterol, which has a similarly hydrated headgroup, fails to increase TE. (B) The chemical structure of PC-cholesterol.